MRS Advances © 2017 Materials Research Society
DOI: 10.1557/adv.2017.303

Rapid elemental composition analysis of intermetallic ternary nanoalloys using calibration-free quantitative Laser Induced Breakdown Spectroscopy (LIBS)

Seyyed Ali Davari[1,2], Sheng Hu[1,3], Erick L. Ribeiro[1,3], and Dibyendu Mukherjee*[1,2,3]

[1] Nano-BioMaterials Laboratory for Energy Energetics & Environment (nbml-E[3]), University of Tennessee, Knoxville, TN 37996, USA;
[2] Department of Mechanical, Aerospace, and Biomedical Engineering, University of Tennessee, Knoxville, TN 37996, USA;
[3]Department of Chemical & Biomolecular Engineering, University of Tennessee, Knoxville, TN 37996, USA

ABSTRACT

Intermetallic ternary nanoalloys (NA) have increasingly gained prominence as excellent catalysts. But, their size, morphology and chemical compositions affect their catalytic and interfacial activities significantly. In this study, we present laser-induced breakdown spectroscopy (LIBS) for rapid quantitative elemental composition characterization of ternary NAs with different elemental ratios. Specifically, we use a calibration-free approach with LIBS to estimate the elemental ratios of PtCuCo ternary NAs with various stoichiometric ratios synthesized via our in-house laser ablation synthesis in solution-galvanic replacement reactions (LASiS-GRR) technique. The size and morphology of the samples are determined from transmission electron microscopy (TEM) and energy dispersive X-ray spectroscopy (EDX) measurements. The LIBS quantitative estimations for the NA samples are compared with results from inductively coupled plasma-optical emission spectroscopy (ICP-OES). The elemental ratio results of quantitative LIBS show good agreement with ICP-OES results, while being devoid of any external standard requirements or extensive sample preparations.

INTRODUCTION

The demand for sustainable power resources has escalated the development of efficient electrochemical energy conversion and storage systems. Heterogeneous nanocomposites (HNCs) and nanoalloys (NAs) play pivotal roles in catalyzing the corresponding cathodic and anodic reactions in the systems [1-5]. Specifically, for proton exchange membrane fuel cells (PEMFCs), Pt-based binary and ternary NAs have been increasingly researched as efficient yet, cost-effective alternatives to pure Pt as catalysts for the cathodic oxygen reduction reactions (ORR) [2, 6, 7]. To this end, the elemental/composition ratios of such heterogeneous nanostructures can tune the corresponding band shifts and structures, which in turn can influence the reactant/intermediate adsorption energies in Pt-based ternary NAs [2, 3]. Thus, rational design of these NA catalysts demand detailed quantitative characterization of their elemental compositions in an efficient and accurate manner.

Laser Induced Breakdown Spectroscopy (LIBS) is a relatively non-destructive spectrochemical characterization technique that involves the collection and processing of spectral emissions emanating from micro-plasma generated by a focused high-irradiance pulsed laser ablating the analyte of interest [8]. The constituents and properties of the plasma bear spectral fingerprints for the sample composition as obtained from the emissions. In recent years, LIBS has been effectively employed for various analytical studies involving combustion [9], and

environmental/bio-hazard analysis [10], pharmaceutical [11], and biomedical [12] applications. Till date, LIBS has largely been recognized as a well-established analytical tool for bulk material characterizations. To this end, only a handful of investigations have reported the use of LIBS for metal/intermetallic NPs including iron oxide nano-powders/NCs [13, 14], Al nanoparticles [15] and Pt based nanocatalysts [16].

In this article, various PtCuCo ternary alloys were synthesized using Laser Ablation Synthesis in Solution-Galvanic Replacement Reaction (LASiS-GRR) technique developed in our laboratory. While their structural properties were confirmed by TEM and EDX, LIBS was employed for quantitative estimation of elemental ratios of the PtCuCo ternary alloys and the results compared with ICP-OES.

EXPERIMENTAL DETAILS

All NA samples for the present study were synthesized using our recently developed LASiS-GRR technique described elsewhere [2]. Briefly, the PtCuCo NAs are synthesized by ablating Co targets with a pulsed laser (1064 nm; 10 Hz with 360 mJ/pulse energy and 4 ns pulse width) in a mixture of K_2PtCl_4 and CuCl solutions. The colloidal solutions are then treated with HCl acid at pH2 for 12 hours followed by centrifugation at 4700 rpm for 8 mins. The resultant samples (precipitates) are marked as PtCuCo-1, PtCuCo-2, and PtCuCo-3 respectively. Finally, the precipitates from centrifugation are collected and deposited on silicon wafers that are pre-washed with water and ethanol to remove any residues for LIBS analyzation. Specifically, around 10 µl of the NP colloidal solutions are drop-caste on Si substrates to result in the material loading densities of 1mg/cm^2 for all the samples. All LIBS measurements are carried out in ambient conditions that facilitate simple and easy execution of the experiments. The LIBS set-up has been described in our earlier works [16]**.**

LIBS methodology

Atomic transition lines are chosen from the NIST Atomic Energy Levels Data Center [17] or from other sources otherwise based on the relative lines strength, and transition probabilities. To gain maximum accuracy in our results for each element in the samples the optimum gate delays are determined based on the variations of the signal-to-noise ratio (SNR) as a function of gate delays for the respective elemental species. The SNR is calculated by measuring the peak signal value at the specific wavelength of interest for a spectral line divided by the noise of the spectra. The noise is defined as the root mean square over the baseline (~ over 40 pixel) adjacent to the analyte peak. The optimum-SNR (I_{em}) is used as the effective emission for the population density calculations of the respective atomic species based on the Boltzmann distribution:

$$I_{em} = hc\frac{A_{ki}}{\lambda_{ki}} N_i \frac{g_k}{g_i} \exp\left(-\frac{\Delta E_{ki}}{k_B T_{exc}}\right) \quad (1)$$

where N_i, A_{ki}, λ_{ki}, g_k, g_i are atomic number densities at the lower energy state, Einstein's transition probability, emitted wavelength, and statistical weights for the upper (k), and lower (i) energy states respectively for the specific atomic transition of interest. ΔE_{ki} is the energy difference between the k, and i states, and T_{exc} is the plasma temperature at the optimal gate delays determined for the species of interest. Boltzmann, and Planck's constant are indicated by

k_B (1.38064×10^{-23} m^2 kg/ s^2 K), and h (6.62607×10^{-34} m^2 kg/s) respectively, and c (3×10^8 m/s) is the speed of light in vacuum. The molar ratio for each element is obtained as:

$$R_X = \frac{C_X}{\sum_s C_s} = \frac{\langle N_i^{XI} \rangle}{\sum_s \langle N_i^{SI} \rangle} \quad (2)$$

where $\langle N_i^{XI} \rangle$ is the average population density of element X undergoing transitions of different k levels to the same i level. The validity of Eq. (1), and the linear Boltzmann plot for plasma temperature calculations are based on the local thermodynamics equilibrium (LTE) conditions for the laser-induced plasma, which typically is established beyond 1μs [8].

DISCUSSION

Fig. 1 shows the representative TEM and XRD results for the PtCuCo ternary NAs synthesized using our LASiS-GRR technique. Fig. 1a indicates that the synthesized

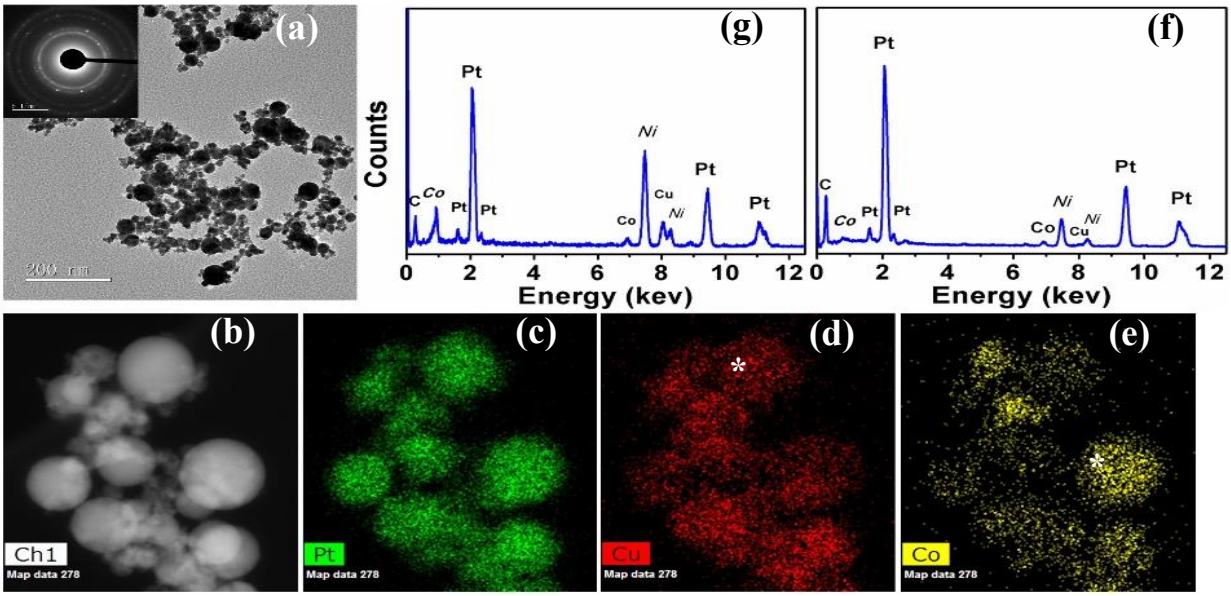

Figure 1. (a) TEM image for the PtCuCo NAs, (b) HAADF image of NA; (c-e) corresponding EDX elemental mappings for Pt, Cu, and Co respectively, (f-g) EDX spectra for the identified spots (*) in (d) and (e) respectively.

ternary NAs are spherical with mean diameter ~20nm. The uniform distribution of Pt, Cu, and

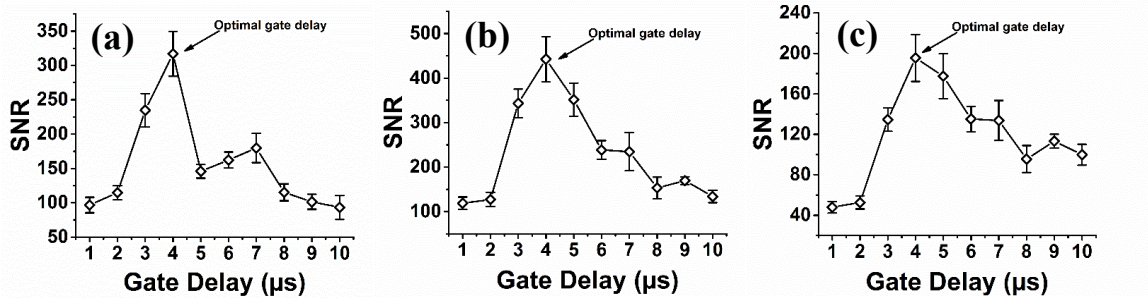

Figure 2. Temporal evolution of SNR from LIBS data for (a) Pt I (306.47nm), (b) Cu I (324.75nm), and (c) Co I (345.35nm). The optimal gate delay for all analytes is determined to be 4 μs.

Table 1. Atomic spectral database [17] for different Pt, Cu, and Co atomic emission lines used for population density calculations.

Species	Wavelength, λ_{ki} (nm)	Transition probability, A_{ki} (10^6 1/s)	Upper energy level, E_k (eV)	Lower energy level, E_i (eV)	g_k	g_i
Pt I[(a)]	265.945	99	4.51086828	0	9	7
Pt I[(a)]	283.02	24	4.23859836	0	7	7
Pt I[(a)]	292.97	22.3	4.0946598	0	7	7
Pt I[(a)]	306.47	67	3.91440216	0	5	7
Cu I	324.754	140	3.816692	0	4	2
Cu I	327.395	138	3.7858976	0	2	2
Co I	340.512	100	4.071888	0.431815	10	10
Co I	345.35	110	4.020881	0.431815	12	10
Co I	350.228	80	3.970904	0.431815	8	10

[(a)] From reference [18]

Co is confirmed through high-angle annular dark-field (HAADF) image and EDX mappings (Fig. 1b-e). Figs. 1f and 1g show the EDX spectra at the identified spots (indicated by * in Figs. 1d and 1e) respectively. The Ni and C peaks in the EDX spectra are resulted from the carbon film with Ni grid. Moreover, comparing the peaks, it can be observed that the amount of Pt is greater than Cu and Co in the synthesized ternary NAs. To quantitatively characterize the elemental ratios in the NA samples, the samples are deposited on silicon wafer for LIBS measurements. Table 1 shows the atomic emission lines used for the population density calculations. The lines are chosen based on their high transition probability, line strength, and lower energy states [17, 18]. To obtain the optimum SNR (I_{em}) for improving the accuracy of quantitative estimations, the temporal evolution of SNR for different emission lines obtained from LIBS are plotted in Fig. 2 as a function of gate delay for a fixed gate width 5 μs. The optimum gate delay for Pt I (306.47nm), Cu I (324.75nm), and Co I (345.35nm) atomic transition lines are determined to be all ~4 μs. The respective spectra of the samples at 4 μs are illustrated in Fig. 3 to indicate the different atomic transition lines of the analyte species of interest. Fig. 3 a & b also indicate a wide range of other detected Pt I transition lines that are

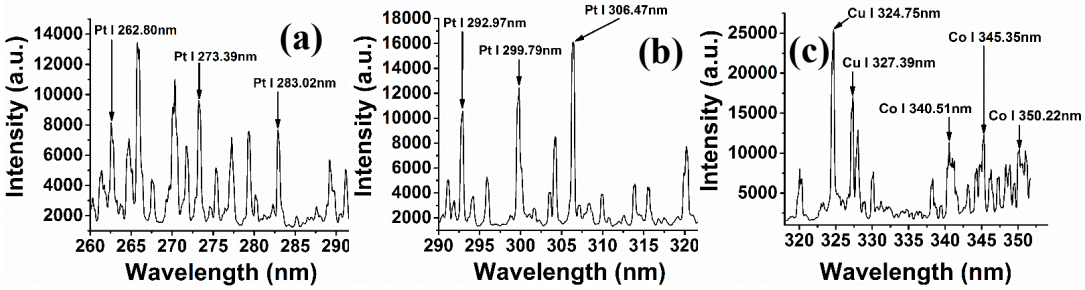

Figure 3. LIBS spectral emission signature from NA samples indicating the various Pt I, Cu I and Co I transition lines collected at 4 μs for the central wavelengths of (a) 275nm, (b) 306nm, and (c) 335nm.

used for constructing Boltzmann plots and plasma excitation temperature calculations. These lines and their properties are listed in the supplementary information. Three different samples with various stoichiometric ratios were prepared using LASiS-GRR technique to generate a wide range of elemental ratios. The plasma excitation temperatures are estimated from the linear fits to the Boltzmann plots obtained from Pt I lines listed in supplementary information (Fig. 4). From the slopes of the fits (R^2 ~0.93 - 0.96), the plasma excitation temperatures are estimated to be 6566.99 ± 776.98 K (PtCuCo-1), 5585.71 ± 772.71 K (PtCuCo-2), and 5108.70 ± 798.27 K

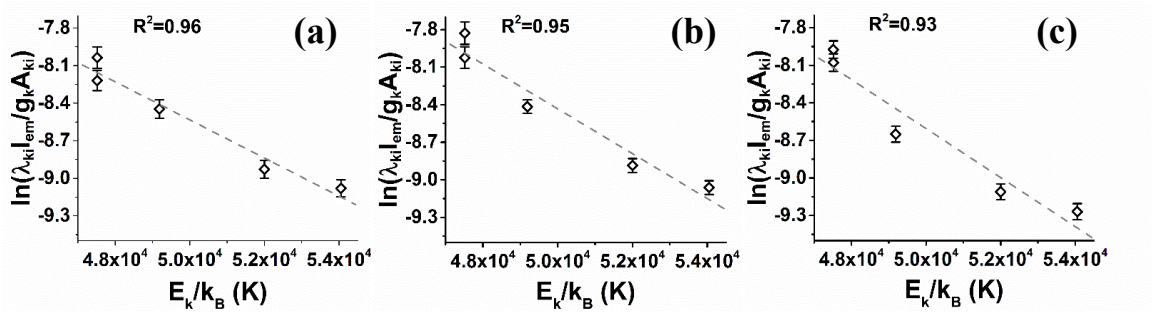

Figure 4. Boltzmann plots and linear fits to calculate the plasma excitation temperature from LIBS analysis of (a) PtCuCo-1, (b) PtCuCo-2, and (c) PtCuCo-3 samples at 4 μs.

(PtCuCo-3) at 4 μs. Upon estimating the plasma excitation temperature, the population densities of various species of interest are calculated and the corresponding estimated molar percentages are reported in Table 2 for the different ternary alloys. Finally, the elemental ratios obtained by LIBS are compared with corresponding results acquired from ICP-OES measurements. Fig. 5 plots the LIBS elemental stoichiometric ratios as a function of ICP-OES results. The ideal match between LIBS and ICP-OES is indicated by the black dashed line. It can be observed that there is a good linear agreement between the two measurement methods. The error bars obtained from the deviations in the population density resulted from different transition lines. A few Cu and Pt molar ratios case specifically for very high ratios of Pt (~0.9 from ICP-OES) and very low ratios of Cu (~0.03 from ICP-OES), as also seen from Table 2, show relatively large deviations from the LIBS results and hence, the detection limitations of LIBS in the extreme cases. The population density depends exponentially on the plasma excitation temperature. Therefore, the uncertainties in the population density can be related to the errors in the plasma excitation temperatures and shot-to-shot variations in the laser-induced plasma. Considering the minimal sample preparation, ease of operation, and no need for standard samples the results acquired by LIBS are satisfactory when compared to ICP-OES measurements.

Table 2. Comparison between elemental ratios obtained from LIBS and ICP-OES.

Samples	Pt		Cu		Co	
	LIBS	ICP-OES	LIBS	ICP-OES	LIBS	ICP-OES
PtCuCo-1	0.70 ± 0.04	0.76	0.17 ± 0.03	0.11	0.13 ± 0.03	0.13
PtCuCo-2	0.74 ± 0.04	0.90	0.19 ± 0.03	0.03	0.07 ± 0.01	0.08
PtCuCo-3	0.71 ± 0.04	0.66	0.22 ± 0.03	0.31	0.07 ± 0.01	0.04

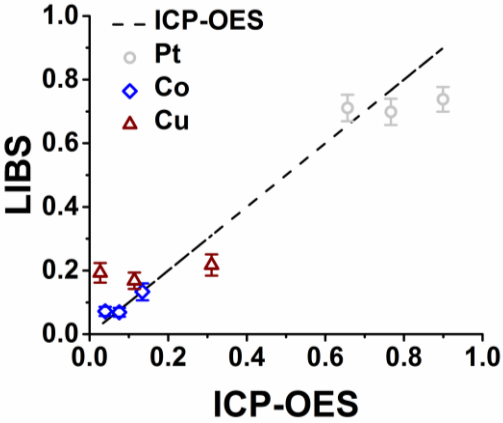

Figure 5. Comparisons between the LIBS and corresponding ICP-OES results. The black dashed line indicates the ideal match.

CONCLUSIONS

Elemental compositions in intermetallic ternary NAs of PtCuCo, synthesized with various stoichiometric ratios via our in-house LASiS-GRR technique, were quantitatively determined using calibration-free LIBS. The population densities for the different analyte species of interest were determined at their lower energy states from the laser-induced plasma analysis based on the Maxwell-Boltzmann relations and the plasma excitation temperatures. This in turn led to the estimation of the respective elemental ratios without the need for any external standards. The LIBS calibration-free results indicated good agreements with those from ICP-OES measurements. The quantitative LIBS methodology presented here mitigates the need for extensive sample preparations, complex operations and external standards, thereby showcasing its advantage over ICP-OES for rapid and robust screening of NA catalytic materials without compromising the accuracy significantly.

REFERENCES

1. S. Hu, C. Melton and D. Mukherjee, Phys Chem Chem Phys **16** (43), 24034-24044 (2014).
2. S. Hu, M. K. Tian, E. L. Ribeiro, G. Duscher and D. Mukherjee, J Power Sources **306**, 413-423 (2016).
3. S. Hu, G. Goenaga, C. Melton, T. A. Zawodzinski and D. Mukherjee, Appl Catal B-Environ **182**, 286-296 (2016).
4. J. A. Scholl, A. L. Koh and J. A. Dionne, Nature **483** (7390), 421-U468 (2012).
5. S. Hu, K. Cheng, E. L. Ribeiro, K. Park, B. Khomami and D. Mukherjee, Catalysis Science & Technology (2017).
6. A. Holewinski, J. C. Idrobo and S. Linic, Nat Chem **6** (9), 828-834 (2014).
7. B. T. Sneed, A. P. Young, D. Jalalpoor, M. C. Golden, S. Mao, Y. Jiang, Y. Wang and C. K. Tsung, ACS Nano **8** (7), 7239-7250 (2014).
8. L. J. Radziemski, T. R. Loree, D. A. Cremers and N. M. Hoffman, Anal Chem **55** (8), 1246-1252 (1983).
9. F. Ferioli, P. V. Puzinauskas and S. G. Buckley, Appl Spectrosc **57** (9), 1183-1189 (2003).
10. D. Mukherjee and M. D. Cheng, J Anal Atom Spectrom **23** (1), 119-128 (2008).
11. D. Mukherjee and M. D. Cheng, Appl Spectrosc **62** (5), 554-562 (2008).
12. S. A. Davari, Masjedi S., Z. Ferdous and D. Mukherjee, J Biophotonics (2017).
13. A. Kebede, A. K. Singh, P. K. Rai, N. K. Giri, A. K. Rai, G. Watal and A. V. Gholap, Laser Med Sci **28** (2), 579-587 (2013).
14. T. Stehrer, B. Praher, R. Viskup, J. Jasik, H. Wolfmeir, E. Arenholz, J. Heitz and J. D. Pedarnig, J Anal Atom Spectrom **24** (7), 973-978 (2009).
15. D. Mukherjee, A. Rai and M. R. Zachariah, J Aerosol Sci **37** (6), 677-695 (2006).
16. S. A. Davari, S. Hu and D. Mukherjee, Talanta **164**, 330-340 (2017).
17. A. Kramida, Ralchenko, Yu., Reader, J. and NIST ASD Team, (2015).
18. E. A. Den Hartog, M. T. Herd, J. E. Lawler, C. Sneden, J. J. Cowan and T. C. Beers, Astrophys J **619** (1), 639-655 (2005).